摘要:本文讨论了具有综合不确定源的多能建筑微电网(MEBM)的双层协调运行方案。首先，提出了考虑电池退化、实际/详细热负荷和各种家用电器运行任务的建筑模型。其次，为了缓解电力需求、冷却水温度、室外温度、居住者新陈代谢、太阳辐照度等多种不确定性因素的不利影响，采用了充分利用历史数据的双层模型，并对求解进行了保守性管理。第一层是sh-g - pmt - y-h。它决定了异构储能资产的调度、多能需求响应以及冷热电联产(CCHP)电厂全天每小时的开关状态。第二层按顺序完成热电转换装置、热电联产装置的运行，以及MEBM和公用电网之间每小时的电力交易，并实现不确定性。数值算例研究表明，该方法具有较高的计算性能和对不确定性的免疫力，能够有效地获得经济的MEBM操作。关键词:电池退化，需求响应，随机加权鲁棒优化，多能建筑微电网，实用热建模。

Stochastic-Weighted Robust Optimization Based Bilayer Operation of a Multi-Energy Building Microgrid Considering Practical Thermal Loads and Battery Degradation

Zhengmao Li, *Member, IEEE*, Lei Wu, *Senior Member, IEEE*, Yan Xu, *Senior Member, IEEE*, and Xiaodong Zheng, *Member, IEEE*

***Abstract*—This paper discusses a bilayer coordinated operation scheme for the multi-energy building microgrid (MEBM) with comprehensive uncertainty sources. First, a building model considering the battery degradation, practical/detailed thermal loads, and various operating tasks of residential appliances is presented. Second, to alleviate the adverse effects from diverse uncertainties of electricity demands, cooling water temperature, outdoor temperature, occupants' metabolism as well as solar irradiance, a bilayer model is applied which makes full utilization of historical data and manages the solution conservativeness. The first layer is the stochastic-weighted robust optimization-based day-ahead operation. It determines the dispatch of heterogeneous energy storage assets, multi-energy demand response, and on-off status of combined cooling, heat and power (CCHP) plants on an hourly basis for the entire day. The second layer sequentially finalizes the operation of the power-to-thermal conversion unit, CCHP plant, and electricity transactions between the MEBM and utility grid hourly with uncertainty realizations. Numerical case studies demonstrate the effectiveness of the proposed approach in obtaining the economic MEBM operation with the high comput-ational performance and immunizing against uncertainties.**

***Index Terms*—Battery degradation, demand response, stochastic-wighted robust optimization, multi-energy building microgrid, practical thermal modeling.**

NOMENCLATURE

Abbreviations

ACF	Average cost for all feasible realizations.
AOP	Alternating optimization procedure.
BEMS	Building energy management system.
BS	Battery storage.
C&CG	Column and constraint generation.
CCHP	Combined cooling, heat and power.
CD	Clothes dryer.
DoD	Depth of discharge.
DR	Demand response.
DW	Dishwasher.
EK	Electric kettle.
EV	Electric vehicles.
FLC	First-layer cost.
HSRO	Hybrid stochastic and robust optimization.
INR	Infeasibility ratio.
IR	Ironing machine.
LOT	Total length of operation time.
LP	Linear programming.
MEBM	Multi-energy building microgrid.
MEP	Multi-energy photovoltaic.
MILP	Mixed-integer linear programming.
MW	Microwave oven.
OW	Operation window.
POT	Preferred operation time.
PtC	Power-to-thermal conversion.
PV	Photovoltaic cell.
RC	Rice cooker.
RO	Robust optimization.
RP	Rated power.
SP	Stochastic programming.
ST	Solution time.
SWRO	Stochastic-weighted robust optimization.
TO	Toaster.
TS	Thermal storage.
V2G	Vehicle-to-grid
VC	Vacuum cleaner.
WM	Washing machine.

Parameters

$^*/\times$	General symbol for appliances.
$a_\ni$, $b_\ni$, $c_\ni$, $k_\ni$	Parameters to model the BS degradation.
$A_{BH}/A_{BW}/A_{PV}$	Area of building envelope/south wall/solar panel.

Manuscript received April 25, 2021; revised September 5, 2021 and October 9, 2021; accepted November 6, 2021. Date of publication November 9, 2021; date of current version March 22, 2022. Paper no. TSTE-00434-2021. *(Corresponding author: Lei Wu.)*

Zhengmao Li and Lei Wu are with ECE Department, Stevens Institute of Technology, Hoboken, NJ 07030 USA (e-mail: zli161@stevens.edu; lei.wu@stevens.edu).

Yan Xu is with Nanyang Technological University, Singapore 639798, Singapore (e-mail: eeyanxu@gmail.com).

Xiaodong Zheng is with the School of Electrical Engineering, Xi'an Jiaotong University, Xi'an 710049, China, and also with the Electric Power Research Institute of China Southern Power Grid Company Ltd., Gaungzhou 510663, China (e-mail: eezhengxd@xjtu.edu.cn).

Color versions of one or more figures in this article are available at https://doi.org/10.1109/TSTE.2021.3126776.

Digital Object Identifier 10.1109/TSTE.2021.3126776

C_{AR}/C_{WA} Thermal capacity of air/water.
E^{*} Total energy requirement of appliance*.
E_{EV}^{in}/E_{EV}^{out} Initial/terminal energy in EV.
$E_{EV}^{min}/E_{EV}^{max}$ Minimum/maximum energy in EV.
$E_{\mathfrak{z}}^{rate}/F_{\mathfrak{z}}^{in}/L_{\mathfrak{z}}^{rate}$ Rated capacity/capital cost/rated life cycle of $\mathfrak{z}$.
H_{BM}^{t} Occupants' metabolism.
H_{TLB}^{t}/H_{HWB}^{t} Basic space thermal/hot water demands.
I_{LE} Gap length of the door or window crack.
K_{HT} Heat transfer coefficient of the room.
N_{T} Total number of dispatch periods.
$P_{BC}^{max}/P_{BD}^{max}$ Maximum BS charging/discharging power/energy.
$P_{BY}^{max}/P_{SE}^{max}$ Maximum purchasing/selling power.
$P_{EL}^{max}/Q_{TL}^{max}$ Maximum allowed electrical/thermal energy.
P_{PtC}^{max} Maximum power consumption of PtC unit.
$E_{BS}^{min}/E_{BS}^{max}$ Minimum/maximal BS energy.
$P_{EC}^{max}/P_{ED}^{max}$ Maximum EV charging/discharging power.
$P_{MT}^{min}/P_{MT}^{max}$ Minimum/maximum power output of CCHP plant.
P_{*}^{rate}/N^{*} Rated power/required LOT of appliance$*$.
P_{PV}^{t}/P_{SL}^{t} Base/stochastic electricity loads.
$Q_{TC}^{max}/Q_{TD}^{max}$ Maximum TS absorbing/releasing power.
$Q_{TC}^{min}/Q_{TD}^{min}$ Minimum TS absorbing/releasing power.
$E_{TS}^{min}/E_{TS}^{max}$ Minimum/maximum TS energy.
R_{MT}^{max} Maximal ramp rate of CCHP plant.
S_{ID}^{t} Solar irradiance.
t 调度间隔的索引。 Index of dispatch intervals.
$T_{IN}^{max}/T_{HW}^{max}$ Maximum indoor/hot water temperature.
$T_{IN}^{min}/T_{HW}^{min}$ Minimum indoor/hot water temperature.
$T_{IN}^{set}/T_{HW}^{set}$ Pre-defined indoor/hot water temperature.
$T_{\mathfrak{z}}^{t}/T_{OT}^{t}/T_{CW}^{t}$ Ambient/outdoor/cold water temperature.
V_{CL} Air volume that infiltrates into the room per meter.
V_{RB}/V_{CW}^{t} Room/cold water volume.
α^{*}/β^{*} Starting/ending time of appliance$*$.
$\alpha_{BH}/\delta_{CN}/\gamma_{it}$ Correction factor for the building envelopes/ cracks/intrusion thermal loss.
$\tau_{EV}/\tau_{BS}/\tau_{TS}$ Self-decay rate of the EV/BS/TS.
δ_{cx}/δ_{jx} Correlation factors for wind blow/building height.
Δt Unit dispatch interval.
η_{BI} Absorption efficiency of solar irradiance by the wall.
$\eta_{MT}^{e}/\eta_{MT}^{h}/\eta_{MT}^{c}$ Power/heat/cooling efficiency of CCHP plant.
$\eta_{PtC}^{h}/\eta_{PtC}^{c}$ Heat/cooling efficiency of PtC unit.
$\eta_{PV}^{p}/\eta_{PV}^{q}$ Electrical/thermal efficiency of MEP system.
η_{BC}/η_{BD} Charging/discharging efficiency of the BS.
η_{TC}/η_{TD} Absorbing/releasing efficiency of the BS.
η_{EC}/η_{ED} Charging/discharging efficiency of the EV.
ξ_{BP}/ξ_{SP} Electricity purchasing/selling prices.
$\xi_{BS}/\xi_{TS}/\xi_{EV}/\xi_{*}$ Unit maintenance cost of EV/BS/TS /appliance$*$.
ξ_{ME}/ξ_{MB} Unit emission cost of CCHP plant/utility grid.
ξ_{NG} Unit price of natural gas fuel.
$\xi_{PV}/\xi_{MT}/\xi_{PtC}$ Unit maintenance cost of MEP system/CCHP plant/PtC unit.
ξ_{MT}^{up} Unit start-up cost of CCHP plant.
ρ_{AR}/ρ_{WA} Air/water density.
$\mathfrak{z}$ General symbol for BS/EV.

Variables

$C_{PV}^{t}/C_{MT}^{t}/C_{PtC}^{t}$ Thermal generation from MEP system/CCHP plant/PtC units.
C_{TD}^{t}/C_{TD}^{t} Absorbing/releasing cooling power of TS.
$\mathrm{DoD}_{\mathfrak{z}}^{t}/L_{\mathfrak{z}}^{t}$ DoD/life cycle of battery $\mathfrak{z}$.
$E_{\mathfrak{z}}^{t}/F_{\mathfrak{z}}^{t}$ Energy stored/degradation cost of battery $\mathfrak{z}$.
F_{BS}^{t}/F_{EV}^{t} Degradation cost of BS/EV.
F_{FC}^{t}/F_{DG}^{t} Fuel/total degradation cost.
F_{OM}^{t}/F_{EM}^{t} Maintenance/emission cost.
F_{ST}^{t}/F_{EX}^{t} Start-up/electricity transaction cost.
H_{PV}^{t}/C_{PV}^{t} Heat/cooling output of MEP system.
H_{BH}^{t}/H_{AH}^{t} Base thermal transfer/additional thermal loss.
H_{CN}^{t}/H_{CR}^{t} Infiltration/intrusion thermal loss.
H_{HW}^{t}/H_{TL}^{t} Hot water/space thermal demands.
H_{MT}^{t}/C_{MT}^{t} Heat/cooling outputs of CCHP plant.
H_{PtC}^{t}/C_{PtC}^{t} Heat/cooling outputs of PtC unit.
$H_{PV}^{t}/H_{MT}^{t}/H_{PtC}^{t}$ Thermal generation from MEP system/CCHP plant/PtC units.
H_{SI}^{t} Heat gain from the solar irradiance.
H_{TD}^{t}/H_{TD}^{t} Absorbing/releasing heat power of TS.
$P_{BC}^{t}/P_{BD}^{t}/E_{BS}^{t}$ BS charging power/discharging power/energy.
P_{BY}^{t}/P_{SE}^{t} Purchasing/selling power.
$P_{EC}^{t}/P_{ED}^{t}/E_{EV}^{t}$ EV charging power/discharging power/energy.
P_{MT}^{t} Power output of CCHP plant.
P_{PV}^{t}/Q_{PV}^{t} Power/thermal generation from MEP system.
$Q_{TC}^{t}/Q_{TD}^{t}/E_{TS}^{t}$ TS absorbing power/releasing power/energy.
T_{HW}^{t}/T_{IN}^{t} Water tank/indoor temperature.
U_{*}^{t}/P_{*}^{t} On-off status/power output of appliance$*$.

I. Introduction

ACCORDING to the report released by the International Energy Agency [1], buildings are showing a globally sharp increase in both carbon emission and energy use. Apart from the prominent electric energy consumption, buildings also host a significant amount of thermal (heat and cooling) loads. With this, advanced technologies, such as the combined cooling, heat and power (CCHP) plants, heterogeneous energy storage assets, power to thermal conversion (PtC) units, photovoltaic cells (PV), etc., are being deployed in buildings to improve the holistic energy efficiency and dispatch flexibility. Under this circumstance, buildings contain sources and loads of multiple

我的介绍。根据能源署[1]的报告，全球建筑物的碳排放和能源消耗都在急剧增加。除了显著的电能消耗外，建筑物还承载了大量的热(热和冷)负荷。因此，先进的技术，如冷热电联产(CCHP)电厂、异构储能资产、电力到热转换(PtC)机组、光伏电池(PV)等，正在被部署在建筑物中，以提高整体能源效率和调度灵活性。在这种情况下，建筑物包含多个源和负载根据国际社会发布的报告

能量形成并呈现多能流的复杂相互作用，形成多能建筑微电网(mebm)[2]。因此，制定实用、全面的MEBM运行模型，以应对发电和用电双方的各种不确定性，获得灵活的运行方案，成为研究热点。

研究人员在设计最优建筑能源管理系统(BEMS)方面做了很多努力[2]。参考[3]研究了MEBM的结构和参数，在考虑多种能源需求、天气条件和能源电价的情况下，研究发电机和储能资产的最优调度。文献[4]提出了一种基于博弈的成本和排放效益分配合作方法，确保城市能源网络中各个mebm能够平等分享效益。[5]中的作者利用建筑物的需求和发电量预测，采用纳什博弈，以最小的成本得出发电机和电池储能(BS)的最优运行决策。尽管在[3]-[5]对于获得具有成本效益的运行方案，它们只关注发电侧的最优多能协调。然而，随着智能电表、控制器、传感器等的部署越来越多，建筑物可以积极参与多种能源需求响应(DR)计划[6]。这些DR方案可以帮助降低能源账单，充分利用用户侧能源，并在平衡可再生能源、延迟网络投资和转移峰值负荷方面支持MEBM运行[7]。从这个意义上说，[3]-[5]的研究未能获得更灵活、更实用的mebm运行方案，而从消费端充分探索多能相互作用是可以实现的。

energy forms and present a complex interplay of multi-energy flows, forming multi-energy building microgrids (MEBMs) [2]. In this regard, formulating practical and comprehensive MEBM operation models to handle diverse uncertainties from both generation and consumption sides and to obtain flexible operation schemes has received intensive research focuses.

Researchers have devoted many efforts to design optimal building energy management systems (BEMS) [2]. Reference [3] explores the structure and parameters of a MEBM to study optimal dispatches of generators and energy storage assets while considering the characteristics of multi-energy demands, weather conditions, and energy tariffs. Reference [4] proposes a game-based cooperative method for the cost and emission benefit allocation, ensuring that individual MEBMs in an urban energy network could equally share benefits. Authors in [5] utilize the demand and generation predictions of buildings and adopt a Nash game to derive optimal operation decisions for generators and battery storage (BS) with minimum costs. Though studies in [3]–[5] contribute to obtaining cost-effective operation schemes, they merely focus on the optimal multi-energy coordination from the generation side. However, with the increasing deployment of smart meters, controllers, sensors, etc., buildings can actively participate in multi-energy demand response (DR) programs [6]. These DR programs can help reduce energy bills, make full utilization of user-side energy sources, and support MEBM operations in terms of balancing renewables, deferring network investment, and shifting peak loads [7]. In this sense, research in [3]–[5] fails to obtain more flexible and practical operation schemes for MEBMs, which otherwise can be achieved by fully exploring the multi-energy interplay from the consumption side.

As for the comprehensive and accurate DR schemes in the MEBM, the paper [8] presents a multi-objective optimization model for a MEBM with multi-energy DR, BS, and PV, for improving the economic operation and meeting compromising occupants' needs. In [9], optimal DR decisions for all electric appliances in the MEBM are obtained under different price schemes to reduce energy supply costs. The study in [10] puts forward a pricing-based DR scheme for a MEBM with various types of household appliances to reduce energy bills without violating the customers' preference. In [11], a BEMS for the MEBM with the DR function is designed to minimize daily energy costs of all appliances under the real-time and demand-charge tariffs. The research in [12] presents a coordinated operation method for a MEBM with generators, BS, and DR schemes, to get the optimal economic benefits and efficiency.

Studies in [8]–[12] clearly show that DR schemes can reduce energy bills and enhance the MEBM operational flexibility. However, they mainly emphasize the consumption side while lacking sufficient coordination with generation sources. Furthermore, in [3]–[5], the degradation of batteries in BSs and electric vehicles (EV), which is an indispensable factor for modeling the practical operation, is not considered and thus hinders their application in real-world scenarios [13]. More importantly, all the above research assumes the predictions of multi-energy resources and demands are accurate. But due to uncertain weather conditions and random human behaviors, there is a high level of uncertainties on both the multi-energy generation and consumption sides. These uncertainties tend to pose a significant threat to the economy and reliability of the MEMB operation.

In the literature, to deal with uncertainties in MEBMs, the stochastic programming (SP) and robust optimization (RO) methods are commonly applied. In [14], a two-stage stochastic energy management system for a MEBM with PVs, BS, and flexible appliances is proposed to minimize energy bills and immune against uncertainties from PV outputs. Nonetheless, neither the battery degradation nor the multi-energy DR, especially for thermal loads, is comprehensively considered. Reference [15] presents a multi-timescale coordinated BEMS for a MEBM integrated with renewables. It aims to dispatch all the building components in two different timescales and mitigate uncertainties in renewables and loads via the SP approach. The study in [16] presents a stochastic model of the MEBM by considering uncertainties from electrical loads and generations. It minimizes the energy supplying costs under a certain comfort level. References [14]–[16] adopt simplified DR models but fail to consider the distinct characteristics and interdependencies, i.e., the operation sequence among various appliances. In addition, the SP approach in [14]–[16] requires exact probability distributions of uncertainty sources, which in practice are hard to obtain. Moreover, it could lead to overly optimistic decisions as it calculates the expectation of all the generated uncertainty scenarios [17].

For the RO method, reference [18] proposes a robust BEMS to optimally dispatch building components against all the uncertainties in a renewable-integrated MEBM. Nonetheless, its DR models fail to practically describe the interdependences of appliances. In [19], to minimize the daily energy bills of a MEBM and eliminate fluctuations of intermittent PV outputs, a coordinated operation framework is presented to dispatch all deferrable appliances and BSs via the RO approach. Though DR schemes for electric appliances are modeled thoroughly, neglecting the BS degradation and thermal loads makes it hard to be applied practically [13]. In addition, the RO methods which calculate the worst-case decisions under the predefined uncertainty set [17] could be overly conservative, as the worst-case occurrence probability is extremely low [18]–[19]. Thus, using the RO method to design actual operation instructions has a significant concern.

To overcome the shortcomings of SP and RO methods, the distributionally robust optimization (DRO) and the hybrid stochastic and robust optimization (HSRO) approach are then applied in the literature. The DRO minimizes the worst-case expected cost over an ambiguity set, which comprises a family of probability distributions with given support and moments of uncertainty sources. Reference [20] presents a single-layer DRO model for the joint energy and reserve dispatch of bulk power systems with a high renewable energy penetration. The DRO method aims at minimizing the total expected operation cost against the worst-case renewable power distribution. In [21], a single-layer DRO method is introduced to operate the energy hub system considering multimodal forecast errors of PV generations. Reference [22] proposes a single-layer DRO model to determine day-ahead unit commitment solutions in a

coordinated electricity and heat network with uncertain power outputs from renewables. In [20]–[22], the DRO makes full use of limited statistical data and produces less conservative and optimistic results by leveraging the worst expectations over all the distributions. Though effective, the DRO approach is computationally intractable and needs additional moment information such as variance and/or covariance of uncertainty distributions.

As for the HSRO method used in the literature, it leverages the SP and RO approaches to respectively deal with different uncertainty sources. In [23], a single-layer two-stage HSRO model is proposed for scheduling commercial microgrids with 100% renewables against uncertainties. Specifically, the SP method is used to deal with uncertainties from the wind speed, solar radiation, and energy demand, while the RO handles uncertainties from the electricity price. In [24], the optimal operation of an integrated electricity and heat system is obtained via the HSRO method. The SP focuses on uncertainties of the load and wind power, while the RO is used to deal with uncertainty from the electricity price. In [25], a HSRO coordinated power management strategy is proposed to improve the flexibility, reliability, and security indices of a microgrid in the presence of EVs, energy storage, distributed generation, and DR. In the HSRO method, RO is used to model uncertainties of the power load, energy price, power generation from renewables, and EV operation parameters, while uncertainties on the availability/unavailability of internal components are tackled via the SP. Though the HSRO method can be effective for obtaining the reliable and economic operation decision, there are still some concerns: first, the exact probability distributions of some uncertainty sources are still needed which can be hard to obtain in reality [20] and the overly-optimistic solutions with regard to those uncertainty sources would be unavoidable. Second, too-conservative results would still be derived for the RO [22]. Further, there is no direct integration of the SP and RO method, i.e., SP and RO are used to handle different sets of uncertainty factors and they are just directly combined to cover all uncertainties. Finally, the single-layer structure used in the DRO and HSRO methods above fails to reveal practical operation conditions against actual uncertainty realizations.

Given the research gap identified above, this paper studies a bilayer coordinated operation method for a MEBM with the practical models for the multi-energy DR and BS degradation. The stochastic-weighted robust optimization (SWRO) approach is used to handle uncertainties with less conservative and optimistic solutions. Compared with existing research, this paper makes the following contributions:

i) A comprehensive coordinated operation model for the MEBM is proposed. It coordinates both the generation and consumption sides rather than merely focusing on one side as in [3]–[5] and [8]–[12]. Furthermore, the thermal and power energy is also co-dispatched.

ii) A practical and flexible operation model for MEBMs is presented considering the specific models for thermal loads and battery degradation. In addition, interdependencies among various household appliances are rigorously modeled.

iii) The bilayer SWRO method is applied in the MEBM to tackle comprehensive uncertainties from the solar irradiance, occupants' metabolism, cooling water temperature, electricity loads, and outdoor temperature as well as to obtain the optimal solution for the day-ahead and intra-day operation. Different from SP [14]–[16], RO [18]–[19], and HSRO [23]–[25] methods, the SWRO calculates the expected operation cost over all the worst-case uncertainty set scenarios, and it does not need accurate probability distributions of uncertainty sources and can effectively avoid solutions conservativeness. Compared with DRO method [20]–[22], it is much more computationally tractable and requires even less information for the uncertainty distributions. To the authors' best knowledge, the related study on the SWRO method is rather limited in the sliterature.

The rest of this paper is organized as follows: Section II shows the practical MEBM model; Section III presents the coordinated operation model of MEBMs; Section IV describes the proposed bilayer structure; Section V gives the detailed solution process of the SWRO approach; Section VI conducts the case studies, and the paper is concluded in Section VII.

II. Practical Component Models of MEBMs

A MEBM as shown in Fig. 1 is a cluster of micro-sources, storage assets, and loads with coupled electrical and thermal energy flows. It is usually built on the building/home scale, appears on the demand side, and directly supplies energy to all appliances [5]. The communication within the MEBM is fulfilled by its inner BEMS, which includes multiple load aggregators that use smart switches to control appliances and smart meters that connect to the utility grid [26].

On the generation side, both the multi-energy photovoltaic (MEP) system and the CCHP plant can produce electrical and thermal energy, and the PtC unit would further intensify the multi-energy interactions. It is noteworthy that rather than the pure electricity generation from the PV system [8], [21], thermal generation from solar energy is also considered in our MEP system[27]. The heterogeneous energy storage system including the BS and thermal storage (TS) is involved to enhance the dispatch flexibility [15]. When the heat andcooling demands coexist, the thermal steam generated from the CCHP plant, PtC unit, and TS are transferred into heat via the heat recovery unit, and the cooling energy is obtained by injecting the thermal steam into the absorption chiller [17]. Finally, the MEBM is also connected to the utility grid or distribution network for electric energy transactions.

On the consumption side, the flexible electrical and thermal loads are considered in this research, and their operation details are presented as follows.

A. Modeling of Household Electric Appliances

In the MEBM, each appliance has an operation window (OW) $[\alpha^*, \beta^*]$ pre-specified by residents [9]. It is indicated in [15] that the residents' comfort is satisfied if the appliance is operated

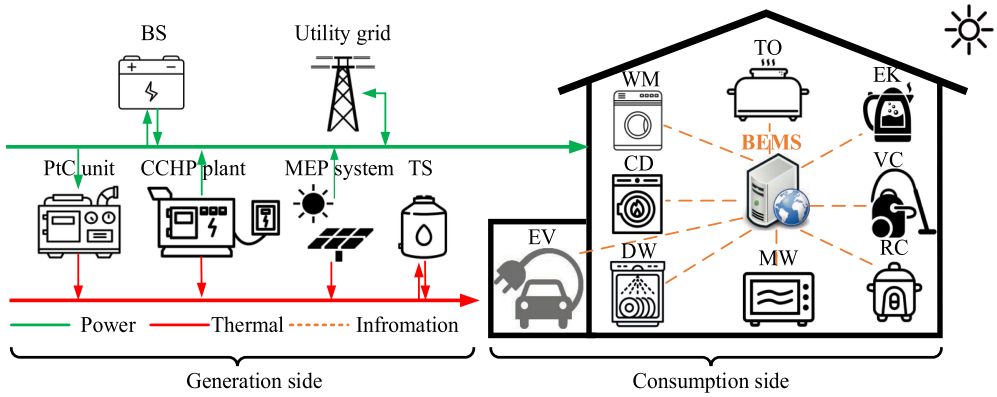

Fig. 1 Typical structure of a house in a MEBM with both generations and loads.

within its OW. In general, those electric appliances can be categorized into the following three categories:

- *Type I: Must-Run Loads:* The base electricity demands, such as lights, refrigerators, etc. that have the fixed energy consumption needs for the MEBM operation.
- *Type II: Stochastic Loads:* The electricity demands resulted from random human behaviors, like personal computers, televisions, hairdryers, etc. These loads are stochastic and may not be forecasted accurately.
- *Type III: Flexible Loads:* Some electric appliances can actively join in DR programs with the assistance of smart meters and financial incentives. By adjusting the operation of these appliances, the total energy bills could be reduced. Specifically, these loads can be classified into two subtypes:

类型:o第三类子类型。i:可中断和可延迟负载:电动汽车就是这种类型的一个例子，它不需要立即(即可延迟)或连续(即可中断)充电操作，只要它可以在OW结束时充电到所需的能量水平。电动汽车的运行约束如(1)-(4)所示。约束(1)描述电动汽车充电功率、放电功率和总储能应在安全范围内;电动汽车的能量演化如(2)所示;约束(3)描述电动汽车在其OW中的初始和终端能量需求;(4)保证电动汽车不同时充放电。

Sub-type III.i: Interruptible & deferrable loads: An EV is an example of this type, which does not need the immediate (i.e., deferrable) or the continuous (i.e., interruptible) charging operation as long as it can be charged to the required energy level by the end of its OW. Operation constraints of an EV are described as in (1)-(4). Constraint (1) describes that the EV charging power, discharging power, and total energy stored should be in their safe ranges; The energy evolution of an EV is described in (2); Constraint (3) describes the initial and terminal energy requirements of an EV in its OW; The non-simultaneous charging and discharging of an EV is guaranteed in (4).

$$[0,0,E_{EV}^{\min}] \le [P_{EC}^t, P_{ED}^t, E_{EV}^t] \le [P_{EC}^{\max}, P_{ED}^{\max}, E_{EV}^{\max}],\ t \in [\alpha_{EV}, \beta_{EV}] \tag{1}$$

$$E_{EV}^t = (1-\tau_{EV})E_{EV}^{t-1} + (P_{EC}^t \cdot \eta_{EC} - P_{ED}^t/\eta_{ED}) \cdot \Delta t,\ t \in [\alpha_{EV}, \beta_{EV}] \tag{2}$$

$$E_{EV}^{\alpha_{EV}-1} = E_{EV}^{in}, E_{EV}^{\beta_{EV}} = E_{EV}^{out} \tag{3}$$

$$P_{EC}^t \cdot P_{ED}^t = 0,\ t \in [\alpha_{EV}, \beta_{EV}] \tag{4}$$

- *Sub-Type III.ii: Non-Interruptible and Deferrable Loads:* Some appliances can shift electricity demands from high electricity price periods to low price periods within a day. Besides, once the appliance starts, it must be finished without interruption. This type of appliance can include the dishwasher (DW), clothes dryer (CD), washing machine (WM), etc. Their operation constraints are described as in (5)-(8) [19]. Constraint (5) means that appliance* will not operate outside its OW. As the electricity consumption of all appliances is usually discrete, when operated, they are in the rated power level as in (6). Constraint (7) indicates that the appliance task shall be completed in the OW. Constraint (8) further enforces that once an appliance is started, all corresponding tasks shall be finished without interruption.

$$U_*^t = 0,\ t \notin [\alpha^*, \beta^*] \tag{5}$$

$$P_*^t = P_*^{rate} U_*^t,\ t \in [\alpha^*, \beta^*] \tag{6}$$

$$\sum_t U_*^t = N_* \ or \ \sum_t P_*^t \Delta t = E_*,\ t \in [\alpha^*, \beta^*] \tag{7}$$

$$\sum_{\tau=t}^{\tau=t+N_*-1} U_*^\tau \ge N_*(U_*^t - U_*^{t-1}),\ \ t \in [\alpha^*, \beta^*] \tag{8}$$

Further, there are certain *interdependencies* among different appliances. For example, although a CD's operation is deferrable, it cannot be operated before a WM completes the task. In this sense, apart from (5)-(8), the following additional constraints shall be enforced for CDs:

Case 1: A CD is used "right" after a WM completes the task (9). Note that '$\times$' indicates the appliance (e.g., CD) which is operated after the appliance* (e.g., WM).

$$\sum_{\tau=t+N_*}^{\tau=t+N_*+N_\times-1} U_\times^\tau \ge N_\times(U_*^t - U_*^{t-1}),\ t \in [\alpha^*, \beta^*] \tag{9}$$

Case 2: A CD can be used "any time" after a WM completes the task, as long as within its OW (10).

$$\sum_{\tau=t+N_*}^{\tau=\beta_\times} U_\times^\tau \ge N_\times(U_*^t - U_*^{t-1}),\ t \in [\alpha^*, \beta^*] \tag{10}$$

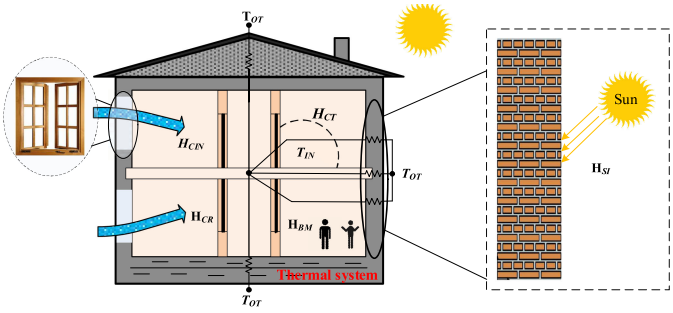

Fig. 2 Typical structure of a room in a MEBM.

B. Practical and Comprehensive Thermal Modelling

In the literature, the thermal demand modelling for buildings and homes is rather simple and coarse [12], [15], [18], which cannot fully describe thermal demands in real-world applications. In this light, a more comprehensive and practical thermal load modelling is conducted in this study.

In the MEBM, a typical structure of a room with thermal loads is shown in Fig. 2. There are two main types of thermal loads: space thermal demands (for maintaining a comfortable room temperature) and hot water demands (for showering and washing needs) [18]. Specifically, in summer, cooling energy is needed for space thermal demands while heat energy is for hot water demands, and in winter, both thermal demands consume the heat energy. Considering that the thermal energy changing rate is much lower than the electric energy due to large thermal inertia [29] and the occupants' tolerance to a reasonable temperature change, thermal demands are regarded as flexible and shiftable. Practical dynamic thermal demand models considering thermal inertia are given below.

- *Space Thermal Demands:* Space thermal demands in Fig. 2 are modelled as follows [30].
  - *Thermal Demand Classification:* The space thermal demand mainly comes from the compensation of thermal losses to maintain suitable room temperature. Total thermal demands can be calculated as in (11). H^t_{BH} (12) includes the heat transfer from all kinds of building envelopes such as doors, walls, floors, etc; H^t_{AH} (13) is the loss resulted from the wind blow and the height of the building; H^t_{CN} (14) means the thermal demands to heat the cold air (in winter) or cool the hot air (in summer) leaking from outside through the door or window cracks; H^t_{CR} (15) describes the thermal demands that heat the cold air (in winter) or cool the hot air (in summer) from casual openings of doors or windows; H^t_{SI} (16) is the heat gain from solar irradiation via building walls. Note that in (11), H^t_{BM} is stochastic given uncertain human behaviors. Besides, H^t_{BM} is thermal loads for summer days while it is the thermal generation for winter days.

$$H^t_{TL} = H^t_{BH} + H^t_{AH} + H^t_{CN} + H^t_{CR} \pm H^t_{SI} \pm H^t_{BM} \tag{11}$$

$$H^t_{BH} = \alpha_{BH} K_{HT} A_{BH} \left| T^t_{IN} - T^t_{OT} \right| \tag{12}$$

$$H^t_{AH} = H^t_{BH} \cdot (\delta_{cx} + \delta_{jx}) \tag{13}$$

$$H^t_{CN} = \delta_{CN} I_{LE} V_{CL} \left| T^t_{IN} - T^t_{OT} \right| \tag{14}$$

$$H^t_{CR} = H^t_{BH} \gamma_{it} \tag{15}$$

$$H^t_{SI} = \eta_{BI} A_{BW} S^t_{ID} \tag{16}$$

  - *Thermal Inertia-Based Load Modelling:* According to the first law of thermodynamics, space thermal demands (11) can be formulated as a dynamic model [29] with the temperature change as in (17).

$$C_{AR}\rho_{AR}V_{RB}dT^t_{IN}/dt = C^t_{PV} + C^t_{MT} + C^t_{PtC} + C^t_{TD} - C^t_{TC} - H^t_{TL} \tag{17}$$

- *Hot Water Demands:* For the water tank, it is assumed to be always full, i.e., the consumed hot water is substituted with the same volume of cold water. The hot water demands given the cold-water volume can be calculated as in (18) [30]. As the inlet cooling water temperature is uncertain, thermal loads from hot water demands are stochastic as well. Still, according to the first law of thermodynamics, temperature of the water tank can be calculated via a dynamic equation as in (19).

$$H^t_{HW} = C_{WA}\rho_{WA}V^t_{CW}(T^t_{HW} - T^t_{CW}), \quad t \in [\alpha_{HW}, \beta_{HW}] \tag{18}$$

$$C_{WA}\rho_{WA}V_{WA}dT^t_{HW}/dt = H^t_{PV} + H^t_{MT} + H^t_{PtC} + H^t_{TD} - H^t_{TC} - C^t_{HW} \tag{19}$$

C. Battery Degradation for BS and EV

The degradation is among the most important factors for practical battery operations. In comparison, as usually the TS is in the form of cheaper thermal tanks, its degradation could be neglected. In some literature, the battery degradation cost is modelled as a linear formulation. For example, in [13], [31], and [32], the linear battery degradation models with regard to the charging and discharging power are proposed for bulk power system and multi-energy microgrid studies. Though their models are simple and computationally friendly, they are overly coarse and cannot accurately quantify the practical battery degradation cost. Hence, a more realistic nonlinear model should be employed.

To evaluate the overall performance of batteries, a key criterion is their life cycle. Taking the lead-acid batteries as an example, their life cycle is mainly dependent on the depth of discharge (DoD) and ambient temperature as in (20) [32], and the DoD of batteries can be denoted as in (21). Using the model proposed by *Kempton* and *Tomic* [33], the degradation cost for batteries is defined as in (22).

$$L^t_ə = (a_ə DoD^t_ə + b_ə) \cdot k_ə \cdot e^{c_ə T^t_ə} \tag{20}$$

$$DoD^t_ə = 1 - E^t_ə / E^{rate}_ə \tag{21}$$

$$F^t_ə = F^{in}_ə L^{rate}_ə / (L^t_ə E^{rate}_ə DoD^t_ə) \tag{22}$$

III. Coordinated Operation of MEBMs

The aim of the coordinated MEBM operation is to obtain a both cost-effective and flexible operation scheme under the operation limits of individual components [10], [15].

A. Objective Function

The objective of the MEBM operation is described as in (23)-(29). Equation. (23) denotes the total MEBM operation cost, including the CCHP fuel cost (24), the maintenance cost of generators, storage assets, and appliances in (25), CCHP start-up cost in (26), the degradation cost of BS and EV in (27), the power transaction cost between the MEBM and utility grid in (28), and emission cost related to the CCHP plant operation and electric energy purchased from the utility grid in (29).

$$\min_{\mathbf{P},\mathbf{Q},\mathbf{E},\mathbf{T},\mathbf{H},\mathbf{C},\mathbf{U}} \sum\nolimits_{t\in N_T} F_{FC}^t + F_{OM}^t + F_{ST}^t + F_{DG}^t + F_{EX}^t + F_{EM}^t \tag{23}$$

where

$$F_{FC}^t = \xi_{NG} P_{MT}^t / \eta_{MT}^e \tag{24}$$

$$F_{OM}^t = \begin{bmatrix} \xi_{PV}(P_{PV}^t + Q_{PV}^t) + \xi_{EV}(P_{EC}^t + P_{ED}^t) + \\ \xi_{BS}(P_{BC}^t + P_{BD}^t) + \xi_{TS}(Q_{TC}^t + Q_{TD}^t) + \\ \xi_{MT} P_{MT}^t + \xi_{PtC} P_{PtC}^t + \xi_* P_*^t \end{bmatrix} \tag{25}$$

$$F_{ST}^t \geq 0; \quad F_{ST}^t \geq (U_{MT}^t - U_{MT}^{t-1}) \xi_{MT}^{up} \tag{26}$$

$$F_{DG}^t = (F_{BS}^t + F_{EV}^t)\big|_{\text{correspond to (22)}} \tag{27}$$

$$F_{EX}^t = \xi_{BP} P_{BY}^t - \xi_{SP} P_{SE}^t \tag{28}$$

$$F_{EM}^t = \xi_{ME} P_{MT}^t + \xi_{MB} P_{BY}^t \tag{29}$$

B. Constraints

All operation constraints for the MEBM are listed in (30)-(53). Besides the constraints in (30) for electrical and thermal loads, the constraint (31) calculates the electrical and thermal generation from the MEP system, (32) describes that thermal generation from the MEP system is equal to its total heat and cooling energy generation, and (33) restricts the maximum heat and cooling energy outputs. Constraint (34) gives the ranges for the power consumption/generation of the PtC unit and CCHP plant. The ramp limit of the CCHP plant is denoted as in (35). Constraints (36) and (37) describe the relationship of the heat/cooling energy generation and power consumption/ generation of the PtC unit and CCHP plant. For electricity transactions with the utility grid, the electricity purchasing and selling shall be within their safe limits (38) and be exclusive (39) [15], [19]. Constraints (40)-(42) describe operation limits of the BS, where (40) is the safe range for the BS charging power, discharging power, and energy level; (41) indicates its energy balance; (42) means that the BS cannot charge and discharge at the same time, and the initial and terminal energy levels in BS shall be equal for maintaining the same dispatch flexibility in a daily cycle [29]. Similar to the BS, operation constraints of the TS are listed as in (43)-(45).

Constraint (46) means that the total absorbed or released heat and cooling energy from TS shall be equal to the total thermal energy. Constraint (47) shows the range of the heat and cooling energy from the TS. The power balance constraint is shown in (48). As mentioned in Section II, the MEBM is on the small building or home scale, thus, their internal network constraints can be neglected and the impact on the utility grid can be considered via the power transaction [11]. The system reliability can be sufficiently guaranteed by the power balance in (48) [15], [18]–[19]. The maximum power consumption/ generation of the MEBM at each operation interval shall be no larger than the maximum allowed quantity as in (49). Similar with the electric energy, the total thermal energy generation shall be no larger than the maximum value as in (50). The operation ranges of the room and hot water temperature are given in (51). Besides, the total thermal energy acquired by residents shall be no less than the base one before the DR scheme as in (52)-(53) [29].

$$(1) - (19) \tag{30}$$

$$[P_{PV}^t, Q_{PV}^t] = A_{PV} S_{ID}^t \cdot [\eta_{PV}^p, \eta_{PV}^q] \tag{31}$$

$$Q_{PV}^t = H_{PV}^t + C_{PV}^t \tag{32}$$

$$0 \leq [H_{PV}^t, C_{PV}^t] \leq Q_{PV}^t \tag{33}$$

$$[0, P_{MT}^{\min} U_{MT}^t] \leq [P_{PtC}^t, P_{MT}^t] \leq [P_{PtC}^{\max}, P_{MT}^{\max} U_{MT}^t] \tag{34}$$

$$-R_{MT}^t \Delta t \leq P_{MT}^t - P_{MT}^t \leq R_{MT}^t \Delta t \tag{35}$$

$$[H_{MT}^t, C_{MT}^t] = [\eta_{MT}^h, \eta_{MT}^c] P_{MT}^t \tag{36}$$

$$[H_{PtC}^t, C_{PtC}^t] = [\eta_{PtC}^h, \eta_{PtC}^c] P_{PtC}^t \tag{37}$$

$$[0, 0] \leq [P_{BY}^t, P_{SE}^t] \leq [P_{BY}^{max}, P_{SE}^{max}] \tag{38}$$

$$P_{BY}^t \cdot P_{SE}^t = 0 \tag{39}$$

$$[0, 0, E_{BS}^{\min}] \leq [P_{BC}^t, P_{BD}^t, E_{BS}^t] \leq [P_{BC}^{\max}, P_{BD}^{\max}, E_{BS}^{\max}] \tag{40}$$

$$E_{BS}^t = (1 - \tau_{BS}) E_{BS}^{t-1} + (P_{BC}^t \eta_{BC} - P_{BD}^t / \eta_{BD}) \Delta t \tag{41}$$

$$P_{BC}^t \cdot P_{BD}^t = 0 \, , E_{BS}^0 = E_{BS}^{N_T} \tag{42}$$

$$[0, 0, E_{TS}^{\min}] \leq [Q_{TC}^t, Q_{TD}^t, E_{TS}^t] \leq [Q_{TC}^{\max}, Q_{TD}^{\max}, E_{TS}^{\max}] \tag{43}$$

$$E_{TS}^t = (1 - \tau_{TS}) E_{TS}^{t-1} + (Q_{TC}^t \eta_{TC} - Q_{TD}^t / \eta_{TD}) \Delta t \tag{44}$$

$$Q_{TC}^t \cdot Q_{TD}^t = 0 \, , E_{TS}^0 = E_{TS}^{N_T} \tag{45}$$

$$[Q_{TC}^t, Q_{TD}^t] = [H_{TC}^t + C_{TC}^t, H_{TD}^t + C_{TD}^t] \tag{46}$$

$$0 \leq [H_{TC}^t, C_{TC}^t] \leq Q_{TC}^t, 0 \leq [H_{TD}^t, C_{TD}^t] \leq Q_{TD}^t \tag{47}$$

$$\begin{bmatrix} P_{PV}^t + P_{MT}^t + P_{BY}^t - P_{SE}^t - P_{PtC}^t + P_{BD}^t \\ -P_{BC}^t = P_{\mathrm{BL}}^t + P_{\mathrm{SL}}^t + P_*^t + P_{ED}^t - P_{EC}^t \end{bmatrix} \tag{48}$$

$$P_{\mathrm{BL}}^t + P_{\mathrm{SL}}^t + P_*^t + P_{ED}^t - P_{EC}^t \leq P_{PL}^{\max} \tag{49}$$

$$\begin{bmatrix} H_{PV}^t + C_{PV}^t + H_{MT}^t + C_{MT}^t + \\ H_{PtC}^t + C_{PtC}^t + Q_{BD}^t - Q_{BC}^t \end{bmatrix} \leq Q_{TL}^{\max} \tag{50}$$

$$[T_{HW}^{\min}, T_{IN}^{\min}] \leq [T_{HW}^{t}, T_{IN}^{t}] \leq [T_{HW}^{\max}, T_{IN}^{\max}] \tag{51}$$

$$C_{HW}^{t} \geq C_{HWB}^{t}\big|_{T_{HW}^{t}=T_{HW}^{set}\ for\ (18)} \tag{52}$$

$$H_{TL}^{t} \geq H_{TLB}^{t}\big|_{T_{IN}^{t}=T_{IN}^{set}\ for\ (11)-(16)} \tag{53}$$

C. Model Linearization

With nonlinear terms in constraint (4), (12), (14), (17), (19), (22), (27), (39), (42), and (45), the MEBM operation model (23)-(53) is a nonlinear non-convex problem. In the literature, intelligent algorithms [7], [11]–[12], [14] or nonlinear solvers [15], [18] are usually applied to get the solution. However, intelligent algorithms may be computationally demanding and dependent on initial conditions along with severe convergence concerns [34], while nonlinear solvers cannot guarantee global optimality.

In this regard, with the practical system setting in Section V, linearization/convexification methods are applied to covert the original problem into a mixed integer linear programming (MILP) model, which then can be effectively solved via industry-grade solvers like CPLEX and Gurobi with a much better computational performance [21], [29]. The detailed linearization and convexification procedures are given in the Appendix.

D. Deterministic Compact Form

For the ease of subsequent discussions, the deterministic MEBM operation problem after convexification/linearization is recast in a compact form as in (54)–(55). Vector $\mathbf{x}$ represents binary and continuous variables $\mathbf{U_{MT}}$, $\mathbf{U}^{*}$, $\mathbf{P}^{*}$, $\mathbf{P_{BC}}$, $\mathbf{P_{BD}}$, $\mathbf{E_{BS}}$, $\mathbf{Q_{TC}}$, $\mathbf{Q_{TD}}$, $\mathbf{E_{TS}}$, $\mathbf{P_{EC}}$, $\mathbf{P_{ED}}$, $\mathbf{E_{EV}}$, $\mathbf{H_{TC}}$, $\mathbf{H_{TD}}$, $\mathbf{C_{TC}}$, $\mathbf{C_{TD}}$, $\mathbf{T_{IN}}$, and $\mathbf{T_{HW}}$; Vector $\mathbf{y}$ denotes all the other continuous variables; Vector $\boldsymbol{d}_0$ corresponds to forecasting vectors $\mathbf{S_{ID}}$, $\mathbf{P_{BM}}$, $\mathbf{P_{SL}}$, $\mathbf{T_{CW}}$, and $\mathbf{T_{OT}}$. $\mathbf{c}$ and $\mathbf{b}$ are cost coefficients. χ means the feasible region of $\mathbf{x}$. (55) represents all the constraints. The two sets of variables are classified according to different layers of the SWRO, which are detailed in the next section.

$$\min_{\mathbf{x}\in\chi,\mathbf{y}} \ \mathbf{c}^{T}\mathbf{x} + \mathbf{b}^{\mathbf{T}}\mathbf{y} \tag{54}$$

$$s.t., \mathbf{Ax} + \mathbf{By} \geq \mathbf{f}; \mathbf{Ex} + \mathbf{Fy} = \mathbf{d_0} \tag{55}$$

IV. Bi-Layer Structure of the MEBM Operation

Given diverse uncertainties from both the generation and consumption sides of the electrical and thermal energy, the deterministic operation model (54)–(55) cannot fully describe the actual MEBM operation.

A. Comprehensive Uncertainty Source Classification

In the MEMG operation, the uncertainty sources include:

Solar irradiation: This affects the electrical and thermal generation of the MEP system (i.e., the generation sides of both electrical and thermal energy), and the heat gain of the building (i.e., the consumption side of thermal energy).

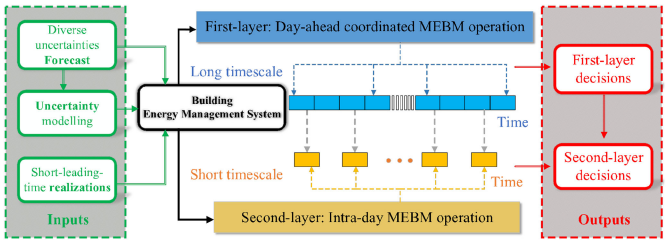

Fig. 3 Bi-layer MEBM coordinated operation framework.

Outdoor temperature: This affects the thermal demands of the building (i.e., the consumption side of thermal energy).

Cooling water temperature: This affects the thermal demands from hot water needs (i.e., the consumption side of thermal energy).

Occupant's metabolism: This affects thermal demands of the building (i.e., the consumption side of the thermal energy).

Stochastic electricity loads: This affects electricity demands (i.e., the consumption side of the electric energy).

It can be seen that compared with other research on optimal operation of building or home microgrids [14]–[16], [18], and [19], uncertainties from both the generation/consumption and power/thermal energy sides are comprehensively considered.

B. Bilayer Coordinated Operation Scheme

To address all the comprehensive uncertainties, a bilayer MEBM coordinated operation framework is designed in Fig. 3.

The first layer is the day-ahead operation. With the full forecast information before the operation, the first layer aims to obtain dispatch decisions for TS, BS, EV, non-interruptible and deferrable appliances, indoor room temperature, hot water temperature, and commitment status of the CCHP plant on an hourly basis for the entire day in one shot (offline). The second layer is intra-day operation. With hourly realizations of all uncertainty sources, it finalizes the multi-energy outputs of the CCHP plant, PtC unit, and electricity transactions between the MEBM and utility grid interval-by-interval (online).

The energy storage assets (e.g., BS, TS and EV) and flexible demands (e.g., electric appliances and thermal-demand-related temperature) take the role of load-leveling/ profit-gaining by making full use of price differences among all dispatch intervals [17]. In this sense, their decisions should be obtained at the first layer, which is given the information for all intervals and runs in one shot. For the unit commitment of the CCHP plant, as it takes time to change its operation status, it is also put in the first layer [15]. As the energy dispatch of the CCHP plant, PtC unit, and power transactions can respond quickly, they are put in the second layer to counteract real-time fluctuations of uncertainty sources.

The two layers are coordinated in the sense that the day-ahead operation decisions are utilized as fixed inputs for the intra-day

operation layer, while intra-day operation constraints are taken into account to derive the day-ahead operation.

V. Solution Process of the SWRO Method

The solution procedure of the proposed bilayer two-stage SWRO coordination model is discussed including uncertainty set modelling, first and second layer operation [18].

A. Uncertainty Modelling

Take solar irradiance as an example, its kth uncertainty set can be formed as in (56). $\sigma_{Id}^{k,dev}$ describes the deviation from the forecast $S_{ID}^{k,fc}$ in the kth uncertainty set. The actual solar irradiance varies between lower and upper limits, while the overall variation is controlled by the pre-specified lower (Γ_{ID}^{min}) and upper (Γ_{ID}^{max}) budget levels [19].

$$\Im_{ID}^{k}=\left\{\mathbf{S}_{ID}^{k}\left|\begin{array}{l}(1-\sigma_{ID}^{k,dev})\le S_{ID}^{t,k}\le(1+\sigma_{ID}^{k,dev})S_{ID}^{k,fc}\\ \Gamma_{ID}^{\min}\le\sum_{t\in N_T,k\in N_K}S_{ID}^{t,k}/\sum_{t\in N_T,k\in N_K}\tilde{S}_{ID}^{t,k}\le\Gamma_{ID}^{\max}\end{array}\right.\right\} \tag{56}$$

Sets and budgets for other uncertainty sources in Section IV can be built similarly.

B. First-Layer: Two-Stage Day-Ahead Operation via SWRO

By leveraging historical data and/or empirical knowledge to reduce the solution conservativeness and the reliance on full uncertainty information, this paper builds a two-stage SWRO model which combines the traditional RO and SP methods for the first layer as in (57)-(60).

$$\min_{\mathbf{x}\in\chi}\ \mathbf{c}^T\mathbf{x}+\mathbf{E}_{\varsigma}[\max_{\mathbf{d}_{\varsigma}\in\Im}\mathbf{L}_{\varsigma}(\mathbf{x},\mathbf{d}_{\varsigma})] \tag{57}$$

$$\text{s.t. } \Upsilon(\mathbf{x},\mathbf{d}_{\varsigma})\neq\emptyset,\quad\forall\mathbf{d}_{\varsigma}\in\Im \tag{58}$$

$$\text{where}\quad \mathbf{L}_{\varsigma}(\mathbf{x},\mathbf{d}_{\varsigma}):=\min_{\mathbf{y}_{\varsigma}\in\Upsilon(\mathbf{x},\mathbf{d}_{\varsigma})}\mathbf{b}^{\mathbf{T}}\mathbf{y}_{\varsigma} \tag{59}$$

$$\Upsilon(\mathbf{x},\mathbf{d}_{\varsigma}):=\{\mathbf{y}_{\varsigma}\,|\mathbf{A}\mathbf{x}+\mathbf{B}\mathbf{y}_{\varsigma}\ge\mathbf{f};\mathbf{E}\mathbf{x}+\mathbf{F}\mathbf{y}_{\varsigma}=\mathbf{d}_{\varsigma}\} \tag{60}$$

Here $\Im$ denotes the collection of all uncertainty sets, indexed by ς; Constraints (59), and (60) denote that the second-stage operation cost $\mathbf{L}_{\varsigma}(\mathbf{x},\mathbf{d}_{\varsigma})$ for a given uncertainty set $\mathbf{d}_{\varsigma}$ is calculated under the first-stage decision $\mathbf{x}$ and constrained on $\Upsilon(\mathbf{x},\mathbf{d}_{\varsigma})$. In (57), within each uncertainty set, uncertainty realizations that maximize $\mathbf{L}_{\varsigma}(\mathbf{x},\mathbf{d}_{\varsigma})$ over the second stage decision $\mathbf{y}_{\varsigma}$ under the given first-stage decision $\mathbf{x}$ can be obtained. In this way, the SWRO method can find a solution that minimizes the first-stage cost and expected worst-case second-stage cost over the collection of all uncertainty sets. Note that with forecasts, the first layer is only conducted once.

The expectation in (57) can be converted into the weighted summation of a credible collection of uncertainty sets with corresponding probabilities as in (61). k and N_K are index and the total number of uncertainty sets. ρ^k is the worst-case probability of uncertainty set k.

It is assumed that uncertainty sets and their corresponding worst-case probabilities for the same uncertainty source could be generated from historical data and/or empirical knowledge.

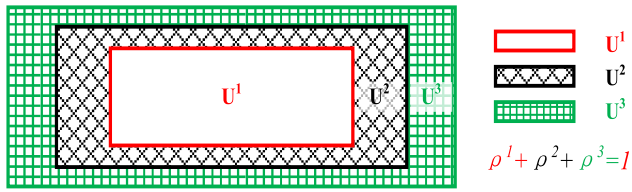

Fig. 4 An illustrative example of three uncertainty sets $\mathbf{U}^1$, $\mathbf{U}^2$, and $\mathbf{U}^3$ with the corresponding worst-case probabilities ρ^1, ρ^2, and ρ^3.

All illustrative example is shown in Fig. 4. In Fig. 4, all the uncertainty sets $\mathbf{U}^1$, $\mathbf{U}^2$, and $\mathbf{U}^3$ are centered on the same point (i.e., forecasts of the uncertainty). Besides, a smaller set is fully included in a larger one, i.e., $\mathbf{U}^1\subset\mathbf{U}^2\subset\mathbf{U}^3$. Finally, the summation of their worst-case probabilities is equal to 1.

Note that the "worst-case probability" is different from the "normal probability" of uncertainty sets. Taking the $\mathbf{U}^3$ as an example, the probability of an uncertainty realization in this set is referred to as the "normal probability", which is 100% in this example. But the occurrence probability of the worst-case realization within $\mathbf{U}^3$, which happens at the boundary of $\mathbf{U}^3$, is denoted as "worst-case probability", which is much smaller than the normal probability in reality [20]. This is also why the RO method is usually regarded as overly conservative [20].

$$\min_{\mathbf{x}\in\chi}\ \mathbf{c}^T\mathbf{x}+\sum\nolimits_{k\in N_K}\rho^k\left[\max_{\mathbf{d}^{\mathbf{k}}\in\Im}\mathbf{L}^{\mathbf{k}}(\mathbf{x},\mathbf{d}^{\mathbf{k}})\right] \tag{61}$$

Proposition 1: The proposed SWRO method would lead to less conservative solutions than the traditional RO method.

Proof 1: Take two uncertainty sets $\mathbf{U}^a$ and $\mathbf{U}^b$ such that $\mathbf{U}^a\subset\mathbf{U}^b$ as an example. Denote their corresponding optimal values of (57)-(60) as θ ($\mathbf{U}^a$) and θ ($\mathbf{U}^a$) obtained by the traditional RO method. That is, θ ($\mathbf{U}^a$) is obtained by considering $\mathbf{U}^a$ only with the worst-case probability $\rho^a=1$, and the same for θ ($\mathbf{U}^b$) with $\rho^b=1$. We have θ ($\mathbf{U}^b$) $\ge$ θ ($\mathbf{U}^a$) as:

$$\theta(\mathbf{U}^b)=\max\left[\theta(\mathbf{U}^a),\theta(\mathbf{U}^b\backslash\mathbf{U}^a)\right] \tag{62}$$

Then, for the SWRO method, we still take $\mathbf{U}^a$ and $\mathbf{U}^b$ for instance but $\rho^a+\rho^b=1$. The optimal value $\Theta[(\mathbf{U}^a,\mathbf{U}^b),(\rho^a,\rho^b)]$ from (57)-(60) can be denoted as:

$$\Theta[(\mathbf{U}^a,\mathbf{U}^b),(\rho^a,\rho^b)]=\rho^a\cdot\theta(\mathbf{U}^a)+\rho^b\cdot\theta(\mathbf{U}^b) \tag{63}$$

Obviously, (64) stands, showing that for the two uncertainty sets, the SWRO is less conservative than the traditional RO method (i.e., only considering the largest set).

$$\theta(\mathbf{U}^a)\le\Theta[(\mathbf{U}^a,\mathbf{U}^b),(\rho^a,\rho^b)]\le\theta(\mathbf{U}^b) \tag{64}$$

The conclusion derived in (64) can be generalized to N_k uncertainty sets. This completes the proof. □

Proposition 2: The proposed SWRO method could lead to less optimistic solutions than the traditional SP method.

Proof 2: If probability distributions of all uncertainty sources are known, the traditional SP formulation can be formed by removing the "max" operator in (57) to get (65). It is obvious the SWRO solution (expectation of all worst cases) is no smaller than the optimal value of (65) (expectation of all optimal cases).

This completes the proof. □

$$\min_{\mathbf{x}\in\chi} \ \mathbf{c}^T\mathbf{x} + \mathbf{E}_\varsigma\left[\mathbf{L}_\varsigma(\mathbf{x},\mathbf{d}_\varsigma)\right] \tag{65}$$

C. Column and Constraint Generation (C&CG) Based Decomposition Algorithm

To solve the two-stage SWRO problem in the first layer, a cutting plane procedure called C&CG is used. In the C&CG, the original SWRO problem is decomposed into one master and one slave problem [18]. To get the final solution, cutting planes described by a set of created recourse decision variables are generated for the master problem. The cutting planes are in the form of recursive constraints obtained from the slave problem. After several iterations of the solution processes, the final optimal solution can be obtained [17].

- *Master Problem:* The master problem can be rewritten in the RO form with recourse actions as follows:

$$\min_{\mathbf{x}\in\chi, L} \ \mathbf{c}^T\mathbf{x} + \eta_S \tag{66}$$

$$s.t., \ \eta_S \geq \sum\nolimits_{k\in N_K} \rho^k(\mathbf{b}^{\mathbf{T}}\mathbf{y}^{\mathbf{k,l}}), \ \ l = 1,2,\ldots,r-1 \tag{67}$$

$$\mathbf{y}^{\mathbf{k,l}} \in \Upsilon(\mathbf{x}, \mathbf{d}_*^{\mathbf{k,l}}), \ \ l = 1,2,\ldots,r-1 \tag{68}$$

where η_S denotes second-stage cost; *r* is the current C&CG iteration and *l* is the index of iterations. $\mathbf{d}_*^{\mathbf{k},l}$ is the worst-case scenario within uncertainty set *k* identified from the slave problem in iteration *l*. The master problem is a MILP model, which derives the first-stage decision $\mathbf{x}^{r*}$.

- *Slave Problem:* The slave problem aims to generate the worst-case scenarios of individual uncertainty sets and obtain an upper bound of (64) by solving the expectation $L_c^r(\mathbf{x}^{r*})$. It is achieved by solving (69)-(70) under the first-stage decision $\mathbf{x}^{r*}$ from the master problem. Given $\mathbf{x}^{r*}$, (69)-(70) could find worst-case uncertainty scenarios $\mathbf{d}_*^{\mathbf{k},r}$ for the current iteration *r* and corresponding second-stage decision $\mathbf{y}^{k,r}$.

$$L_c^r(\mathbf{x}^{r*}) = \left\{ \begin{array}{l} \sum_{k\in N_K} \rho^k \left[\max\limits_{\mathbf{d^k}\in\Im} L^{\mathbf{k}}(\mathbf{x}^{r*})\right] = \\ \sum_{k\in N_K} \rho^k \left[\max\limits_{\mathbf{d^k}\in\Im} \min\limits_{\mathbf{y^k}} \mathbf{b}^{\mathbf{T}}\mathbf{y}^{\mathbf{k}}\right] \end{array} \right\} \tag{69}$$

$$s.t., \ \mathbf{B}\mathbf{y}^{\mathbf{k}} \geq \mathbf{f} - \mathbf{A}\mathbf{x}^{\mathrm{r}*}; \ \ \mathbf{F}\mathbf{y}^{\mathbf{k}} = \mathbf{d}^{\mathbf{k}} - \mathbf{E}\mathbf{x}^{\mathrm{r}*} \tag{70}$$

To reformulate the "maxmin" function (69) in a tractable way, the strong duality [19] is used to equivalently convert the *max-min* problem (69)-(70) as (71)-(72).

$$\sum_{k\in N_K} \rho^k \left[\max_{\mathbf{d^k}\in\Im, \psi^{\mathbf{k}}, \pi^{\mathbf{k}}} \ (\psi^{\mathbf{k},r})^{\mathrm{T}}(\mathbf{f} - \mathbf{A}\mathbf{x}^{\mathrm{r}*}) + (\pi^{\mathbf{k},r})^{\mathrm{T}}(\mathbf{d}^{\mathbf{k}} - \mathbf{E}\mathbf{x}^{\mathrm{r}*})\right] \tag{71}$$

$$s.t., \ \ (\psi^{\mathbf{k},r})^{\mathrm{T}}\mathbf{B} + (\pi^{\mathbf{k},r})^{\mathrm{T}}\mathbf{F} = \mathbf{b}; \ \ \psi^{\mathbf{k},r} \geq 0, \pi^{\mathbf{k},r} \ free \tag{72}$$

where $\psi^{k,r}$ and $\pi^{k,r}$ are the dual variables for inequality and equality constraints in (70).

Algorithm 1: Alternating Optimization Procedure (AOP).

Start with an initialized $\underline{\mathbf{d}}^k \in \Im$ (the initialized $\underline{\mathbf{d}}^k$ could be set as the deterministic forecasts of all uncertainty sources)
Repeat
Solve $(*)$:
$\mathrm{L} \leftarrow \sum_{k\in N_K} \rho^k [\max\limits_{\psi^{\mathbf{k}}, \pi^{\mathbf{k}}} \ (\psi^{\mathbf{k},r})^{\mathrm{T}}(\mathbf{f} - \mathbf{A}\mathbf{x}^{\mathrm{r}*}) + (\pi^{\mathbf{k},r})^{\mathrm{T}} (\underline{\mathbf{d}}^{\mathbf{k}} - \mathbf{E}\mathbf{x}^{\mathrm{r}*})]$
if $\mathrm{L} < \infty$
Let $\underline{\psi}^{k,r}$ and $\underline{\pi}^{k,r}$ be the optimal solutions for $(*)$
Solve $\mathrm{L}' \leftarrow \sum_{k\in N_K} \rho^k [\max\limits_{\mathbf{d^k}\in\Im} \ (\underline{\psi}^{\mathbf{k},r})^{\mathrm{T}}(\mathbf{f} - \mathbf{A}\mathbf{x}^{\mathrm{r}*}) + (\underline{\pi}^{\mathbf{k},r})^{\mathrm{T}}(\mathbf{d}^{\mathbf{k}} - \mathbf{E}\mathbf{x}^{\mathrm{r}*})]$ and let $\underline{\mathbf{d}}^k$ be its optimal solution
else
$\mathrm{L}' = \infty$
end if
Until $\mathrm{L}' = \infty$ or $|\mathbf{L}'\text{-}\mathbf{L}| \,/\, \mathbf{L} \leq \sigma$ where σ is a pre-defined solution gap
Output L' as an estimate of $L_c^r(\mathbf{x}^{r*})$ in (69) with solution $\underline{\mathbf{d}}^k$

Due to the nonlinearity/non-convexity, the dual problem (71) with the bilinear term $(\pi^{k,r})^T\mathbf{d}^k$ is hard to be solved directly. Therefore, the alternating optimization procedure (AOP) can be applied, which decomposes the original nonlinear/non-convex problem (71) into sets of iterative linear ones with a reduced computational burden. The detailed process of the AOP is described in ***Algorithm 1*** [20], [35].

D. Second Layer: Intra-Day Operation

With the optimal day-ahead solutions $\mathbf{x}^*$ obtained from the first-layer model and the updated short-lead time forecasts on uncertainties $\boldsymbol{d}_0$, the second-layer model is formed as a linear programming (LP) problem (73)-(74) to get the final intra-day operation decisions. For the second layer, with updated forecasts, it is conducted multiple times in a successive manner (i.e., hour by hour) [15].

$$L(\mathbf{x}^*, \mathbf{d}_0) : = \min_{\mathbf{y}} \mathbf{b}^{\mathbf{T}}\mathbf{y} \tag{73}$$

$$s.t., \ \ \mathbf{B}\mathbf{y} \geq \mathbf{f} - \mathbf{A}\mathbf{x}^*; \ \ \mathbf{F}\mathbf{y} = \mathbf{d}_0 - \mathbf{E}\mathbf{x}^* \tag{74}$$

E. Holistic Solution Process for the Bilayer SWRO Method

To demonstrate the solution procedure of the proposed bi-layer SWRO method comprehensively, the overall process is described in the flowchart of Fig. 5 [17].

Fig. 5 shows that the first layer mimics the second-layer operation through its second-stage (slave) problem to obtain the day-ahead operation decisions, while decisions for the second layer are finalized with the passing-down of the first layer decisions. In this way, the two layers are coordinated for deriving optimal and practical MEMG operation solutions In addition, as

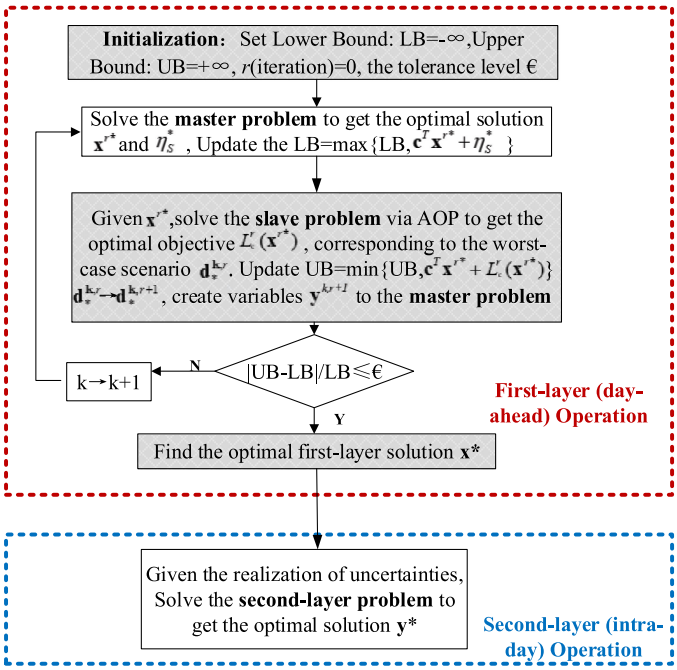

Fig. 5 The flowchart of the bi-layer SWRO method.

TABLE I
KEY OPERATING PARAMETERS FOR GENERATION SIDE [15], [29], [32]

η^{e}_{MT}	η^{h}_{MT}	η^{c}_{MT}	η^{h}_{PtC}	η^{c}_{PtC}
0.29	1.26	1.35	2.75	3.25
η^{p}_{PV}	η^{q}_{PV}	η_{BC}&η_{BD}	η_{TC}&η_{TD}	η_{EC}&η_{ED}
0.15	0.18	0.98	0.95	0.98
P^{max}_{BC} &P^{max}_{BD}	P^{max}_{TC} &P^{max}_{TD}	P^{max}_{EC} &P^{max}_{ED}	E^{min}_{BS}	E^{max}_{BS}
1.3kW	1.6kW	1.35kW	0.8kWh	3.6kWh
E^{min}_{TS}	E^{max}_{TS}	E^{min}_{EV}	E^{max}_{EV}	A_{PV}
0kWh	4.5kWh	1.8kWh	8.1kWh	5m2

TABLE II
PARAMETERS OF THE MEBM [9], [11], [15], [19]

Appliance	OW	LOT	PR (W)	POT
WM	9:00-21:00	2	1000	19:00,20:00
DW	14:00-19:00	2	1000	19:00,20:00
CD	11:00-23:00	1	1800	21:00
IR	17:00-22:00	1	1300	22:00
VC	7:00-9:00; 17:00-22:00	1	900	21:00
MW	7:00-9:00; 11:00-13:00; 17:00-19:00	1	800	12:00
RC	11:00-13:00, 16:00-19:00	2	1000	17:00,18:00
EK	7:00-10:00	1	1000	8:00
TO	7:00-9:00	1	800	7:00

TABLE III
PARAMETERS FOR UNCERTAINTY SETS

Index of uncertainty sets	1	2	3	4	5
Solar irradiance	0.15	0.17	0.18	0.2	0.25
Outdoor temperature	0.08	0.085	0.09	0.095	0.1
Stochastic electricity loads	0.1	0.12	0.13	0.14	0.15
Cooling water temperature	0.08	0.085	0.088	0.09	0.1
Occupations' metabolism	0.15	0.16	0.18	0.19	0.2
Worst-case Probability	0.25	0.2	0.35	0.1	0.1

the first-layer decisions are obtained against the worst cases of all uncertainty sets, as long as the uncertainty realizations in the second layer are within the uncertainty sets, its operation will always be feasible [17], [19].

VI. CASE STUDIES

A grid-tied MEBM with a similar structure in Fig. 1 is applied to verify the effectiveness of our proposed method. The MEBM is located in Tianjin (38° N, 117° E), China. The power and thermal energy capacities of the MEBM are 10kW and 15kW, respectively.

In the MEBM, the room is oriented South with a floor area of 200 (16*12.5) m^2. Areas of north/south and east/west facing walls are 44.8 (16*2.8) m^2 and 35 (12.5*2.8) m^2. South and north walls are equipped with double-glazed windows to the outside environment with areas of 11.2 m^2 and 8.96 m^2. All windows are in the casement type without any blind or shading device. The area of the door on the east side is 2.1 m^2. All the walls and the roof are comprised of the same structural insulated panels [30]. Specific building thermal parameters and hot water demands are given in [36].

On the generation side, there is 1 CCHP plant, 1 PtC unit, 1 MEP system, 1 BS, and 1 TS. The key operating parameters for the generation side are given in Table I. Other parameters are listed in [36]. As for the PLF approximation of the original battery degradation costs of the BS and EV, in this study, 7 blocks are utilized in each PLF to make the tradeoff between the computation time and solution accuracy. The maximal approximation errors of PLFs with regard to the original nonlinear cost are evaluated in [36] and it can be seen that the approximation accuracy is acceptable for the case study.

On the consumption side, apart from the must-run and stochastic electrical demands, other appliances are listed in Table II with their OWs, total length of operation time (LOT), rated power (RP), and preferred operation time (POT).

For EV, the state of charge when it arrives at home is 0.3, and the residents would prefer to optimally charge their battery only during 23:00-3:00, i.e., no vehicle-to-grid (V2G) is allowed during that period.

A summer case is tested, which includes space cooling and hot water as thermal loads. The predefined indoor room and hot water temperature are 75 °C and 25°C, with the ranges of [72, 78] °C and [23, 27] °C.

The forecasts of all the heterogeneous uncertainty sources and their uncertainty set are shown in Fig. 6.

With the historical data, five uncertainty sets are generated. Their uncertainty deviations and worst-case probabilities are given in Table III. It should be noted that the worst-case probability of the largest uncertainty set can be rather low, while the worst-case probabilities for small uncertainty sets are relatively higher. Electricity transaction prices between the MEBM and utility grid are shown in Fig. 7.

For the first layer, the operation horizon is 24 hours with 1-hour granularity; For the second layer, the one-hour ahead operation is done with successively updated short-lead time predictions. Without loss of generality, other real-world data

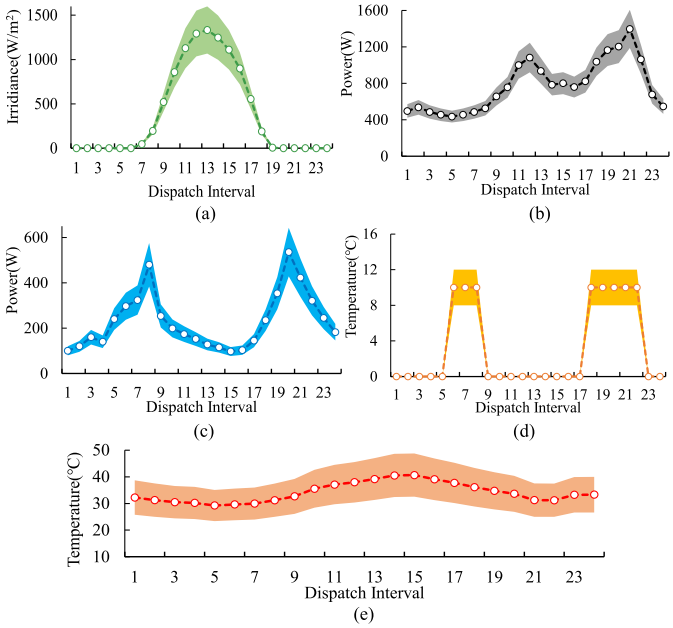

Fig. 6 Deterministic forecast within the maximal uncertainty set.

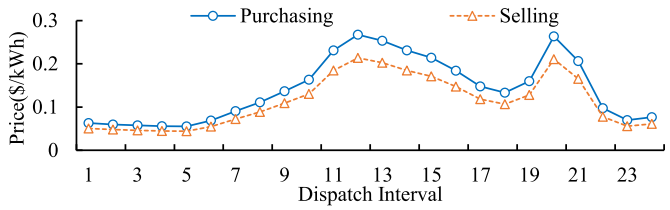

Fig. 7 The electricity transaction prices between the MEBM and utility grid.

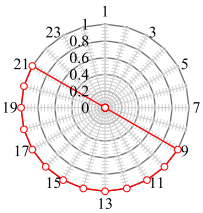

Fig. 8 Unit commitment of CCHP plant.

for the MEBM could also be applied without affecting the effectiveness of our proposed method, as they are just inputs for the SWRO method. Furthermore, this study mainly focuses on the steady-state MEBM operation, thus, dynamic load or generation changes, which could be tackled by emerging control methods [37], are not considered.

All simulations are implemented in an Intel(R) Core(TM) i7-10710U CPU @ 1.10GHz, 1.61 GHz with a 16G memory. The General Algebraic Modelling System (GAMS) platform is utilized to solve the MILP problem with the CPLEX solver.

A. *First-Layer Operation Results*

The optimal commitment status of the CCHP plant is given in Fig. 8. Comparisons of operational decisions for all electric appliances before and after our method are given in Fig. 9(a) and (b), respectively. The electrical load profiles, indoor room temperature, and hot water temperature in the water tank before and after the DR scheme are compared in Figs. 10 –12.

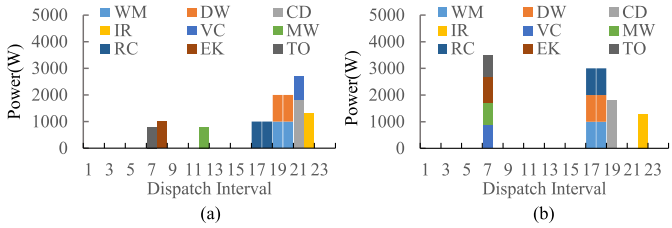

Fig. 9 Operation decisions of the flexible appliances.

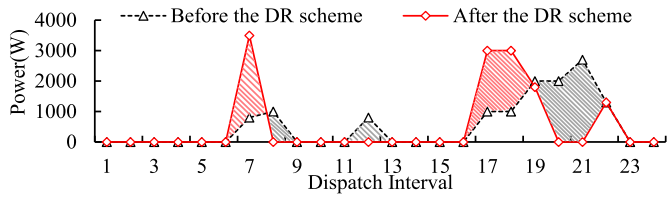

Fig. 10 Load profile comparison for the non-interruptible & deferrable loads.

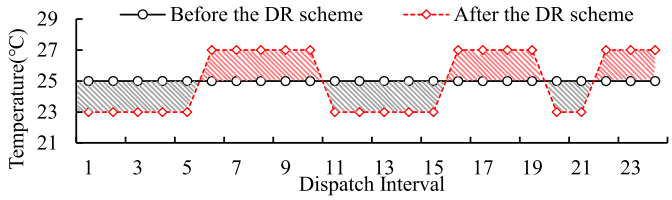

Fig. 11 Indoor room temperature comparison.

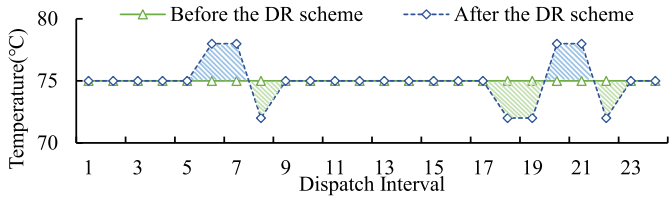

Fig. 12 Hot water temperature comparison.

The figures show that:

i) The CCHP plant, as the main source for multi-energy generation, would operate when the thermal demands and/or electricity transaction prices are high, i.e., at intervals 9-21.

ii) Household appliances are effectively scheduled under the DR scheme: compared with the POT (without DR scheme) of all appliances in Fig. 9(a), appliances are scheduled at intervals with lower electricity prices in Fig. 9(b) within OWs, such as intervals 7, 17–18, 23. In this regard, the MEBM operation cost will be reduced. Besides, the shaded areas in Fig. 10 denote the amount of shifted electrical energy.

iii) The interdependency of appliances is maintained in Fig. 9(b). For instance, the CD is operated right after the completion of the WM. This further shows the effectiveness of our DR scheme.

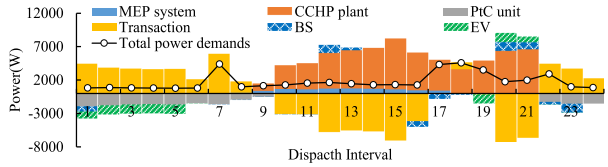

Fig. 13 Power balance condition for the MEBM.

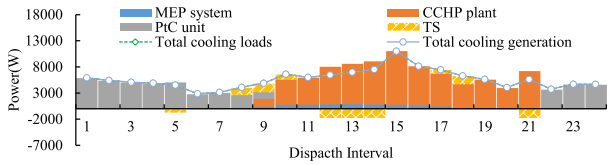

Fig. 14 Cooling balance condition for the MEBM (space cooling).

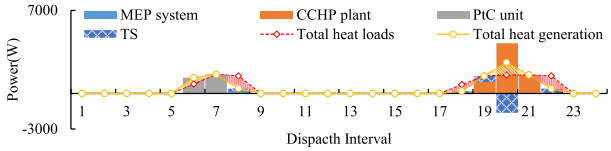

Fig. 15 Heat balance condition for the MEBM (hot water demand).

iv) With flexible temperature ranges (because of the thermal inertia), thermal demands are scheduled effectively. By varying the hot water and indoor room temperature within the pre-defined ranges in Figs. 11 and 12, the thermal demands are shifted to lower energy supplying cost. The shaded area in Figs. 11 and 12 denote part of the shifted thermal energy.

The optimal objective of 7.43$ is obtained in 14.85s, showing the effectiveness of the SWRO in obtaining cost-effective day-ahead operation solutions within the applicable solution time (ST).

B. Second-layer Operation Results

Given realizations of all the uncertainty sources, the second layer operation results are given in Figs. 13 –15. From all the figures, it can be inferred that:

i) From the generation side: All the assets are coordinated for a more flexible and cost-effective multi-energy generation. When the electricity transaction prices are low at intervals 1-9 and 22-24, the thermal energy is mainly generated by the PtC unit, and there is a large amount of electricity purchased from the main gird; When the electricity transaction prices are high at intervals 9-21, most of the electrical and thermal energy is generated from the CCHP plant, and the MEBM also sells electrical energy to the main grid for higher revenue. Further, the BS and TS contribute to shifting the loads and gaining additional profit by coordinating with generators and power transactions with the main grid.

ii) From the consumption side: Our proposed method is effective in making full use of the thermal inertia and scheduling all loads for a more flexible and economic multi-energy consumption. Fig. 13 shows that, rather than only engaging in the charging actions without the DR scheme, EV would charge when the electricity prices are low and discharge at high price intervals. In this sense, EV contributes to making full use of the price information to reduce total energy supply cost and flexiblize the overall operation. Figs. 14 and 15 further show that thermal (heat or cooling) generation and loads are not strictly the same at each time interval. This is because considering thermal inertia, the space air, and hot water can act as TSs to store or release energy for shifting thermal loads and reducing energy bills. The shaded areas in Figs. 14 and 15 are the thermal demands shifted. As the heat capacity of the air is much lower than water, the storage effect for the space air is less prominent than water in Fig. 15.

TABLE IV
METHOD COMPARISON RESULTS

	#M1	#M2	#M3	#M4	#M5
FLC	6.26$	6.27$	7.58$	8.44$	7.43$
First-layer ST	1.62s	1.96s	11.39s	11.55s	14.85s
ACF	6.28$	6.30$	7.50$	8.47$	7.46$
INR	10.8%	10.1%	0	0	0
Second-layer ST	0.12s	0.13s	0.12s	0.13s	0.13s

For the second layer, the finalized MEBM operation cost is 7.46$ and the ST for each interval is only 0.13s, which further shows the computational efficiency of our proposed method.

C. Comparison With Other Operation Benchmarks

The proposed method is further compared with four methods to comprehensively understand its efficacy:

#M1: Deterministic Operation Method: It is assumed that the forecasts of all the uncertainty sources are accurate.

#M2: Traditional SP Method: It is assumed that probability distributions of all uncertainty sources are known. Then, 2,000 scenarios are generated to simulate uncertainties and reduced to 5 representative ones. For our study, there is one scenario generated in each uncertainty set.

#M3: Traditional RO Method: Only the largest uncertainty set, *i.e.*, the first column in Table II, is considered.

#M4: No Multi-Energy DR Scheme Involved: The MEBM does not join in the DR scheme, that is, all the demands are not flexible and V2G is not allowed.

Our method is marked as **#M5** in the following discussions. Besides the first-layer cost (FLC), all the second layers of five methods utilize 1,000 randomly generated uncertainty realizations to check the infeasibility ratio (INR) and the average cost for all feasible realizations (ACF). Simulation results are shown in Table III.

The comparison results in Table IV indicate that:

i) *Considering diverse uncertainties is effective to guarantee a more reliable MEBM operation*: Compared to **#M1**, system uncertainties are all tackled in **#M2-#M5**. Thus, though the FLC of **#M1** is the lowest (cost difference with **#M1** is regarded as the extra cost for handling uncertainties in other methods), it has the largest infeasible rate under the realizations of uncertainties in the second layer.

ii) *Our proposed method can avoid the overly optimistic solution:* Although the FLC of **#M5** is higher than **#M2**, there are infeasible uncertainty realizations in **#M2**. This is

because the scenario generation method will unavoidably lose certain uncertainty information, especially those scenarios that deviate a lot from the forecast with extremely low probabilities. Then calculating the expected cost of those scenarios which are more similar to the forecast in the SP method could be overly optimistic. In this light, it can be seen that the cost of **#M2** is only slightly higher (optimistic) than **#M1**. This also verifies Proposition 2 in Section IV.

iii) *Our proposed method can avoid overly conservative solutions:* Although both **#M3** and **#M5** do not no incur infeasible cases, the FLC and ACF of **#M3** are both higher than **#M5**. This is because only considering the largest (worst) uncertainty set in **#M3** would lead to overly conservative solutions. This also verifies Proposition 1 in Section IV.

iv) *The multi-energy DR scheme could contribute to high cost-saving:* This is prominent by comparing FLC and ACF for **#M4** and **#M5**.

v) *The MILP models of all methods for both the day-ahead and intraday operations are computationally trackable:* For the first layer, as the problem dimension is rather low, STs of **#M1** and **#M2** are short. However, as **#M3**-**#M5** involve numerous iterations from the AOP and C&CG algorithm, their STs are longer than **#M1** and **#M2**. The number of scenarios in **#M2** is four times more than **#M1**, leading to a higher ST. This is also the reason why the STs of **#M4** and **#M5** are higher than **#M3**. Compared with **#M5**, decisions for electric appliances are fixed (no need to be re-optimized) in **#M4**, hence, the ST of **#M5** is longer. For the second layers of all the methods, they are linear optimization problems with short STs. In addition, as the dimensions of their second layer problems are the same, their STs are almost the same. The STs of both layers for all the methods show the computational effectiveness of the MILP model. Thus, the proposed MILP model is compatible with practical applications.

All the simulation results demonstrate that our proposed bi-layer SWRO method can effectively coordinate generation and consumption sides for the more cost-effective MEBM operation and flexible multi-energy coordination with the favorable computational performance.

VII. Conclusion

This paper proposes a bilayer SWRO approach for multi-energy coordination of a smart MEBM under heterogeneous uncertainties. Then, the practical and comprehensive system models from both generation and consumption sides are involved for the more flexible and cost-effective system operation. Numerical case studies are conducted with the following conclusions:

i) The proposed bilayer MEBM model is effective and efficient for a more flexible and cost-effective operation.

ii) Considering the practical multi-energy DR scheme in terms of the operational flexibility and interdependency of the household appliances as well as the thermal inertia contributes to a more flexible and economic multi-energy supply scheme.

iii) The proposed SWRO method could effectively balance solution optimality and conservativeness for the MEBM as compared to the traditional SP and RO based methods.

In the future, on the one hand, the data-driven machine learning based methods could be used to explore the optimal multi-energy operation solutions for emerging smart buildings and homes; On the other hand, the islanded MEBM operation could be studied. Specifically, for the islanded mode without the powerful electricity support from the main grid, the direct load control scheme [37] shall be introduced to mandatorily adjust loads and sustain supply-demand balance.

Appendix: Model Linearization and Convexification

i) *For Differential Equations (17) and (19) in the Thermal Model:* As indoor temperature varies rather slowly due to the large thermal inertia, the hourly state difference model as in (A.1) can be used [29]. A similar transformation for the hot water demands can be conducted.

$$T_{IN}^{t} - T_{IN}^{t-1} = \frac{(C_{MT}^{t} + C_{PtC}^{t} + C_{TD}^{t} - C_{TC}^{t} - H_{TL}^{t})\Delta t}{C_{AR}\rho_{AR}V_{RB}} \tag{A.1}$$

ii) *For the Polynomial Terms in (22) and (27):* The piecewise linear function (PLF) method from reference [17] could be utilized to approximate the original nonlinear one.

iii) *For Absolute Values in (12) and (14):* In fact, the space thermal loads are needed either for space heat (in winter) or cooling (in summer) [30], therefore, these absolute functions can be directly removed according to actual situations.

iv) *For Bilinear Terms in (4), (39), (42), and (45) Describing the Exclusive Actions:* To linearize these bilinear terms, auxiliary binary variables can be introduced as in [29]. Taking the BS operation in (4) for instance: two binary variables can be applied to describe BS charging and discharging statuses, then by limiting the summation of the two status variables to be no larger than one, the exclusive charging and discharging can be guaranteed.

References

[1] IEA, *Global Status Report For Buildings and Construction*, Nairobi, Kenya: IEA, Paris, 2019. [Online]. Available: https://www.iea.org/reports/global-status-report-for-buildings-and-construction-2019

[2] M. A. Hannan *et al.*, "A review of internet of energy-based building energy management systems: Issues and recommendations," *IEEE Access*, vol. 6, pp. 38997–39014, 2018.

[3] M. Szypowski, T. Siewierski, and A. Wędzik, "Optimization of energy-supply structure in residential premises using mixed-integer linear programming," *IEEE Trans. Ind. Electron.*, vol. 66, no. 2, pp. 1368–1378, Feb. 2019.

[4] R. Jing *et al.*, "Multi-objective optimization of a neighborhood-level urban energy network: Considering game-theory inspired multi-benefit allocation constraints," *Appl. Energy*, vol. 231, no. C, pp. 534–548, 2018.

[5] M. H. K. Tushar, A. W. Zeineddine, and C. Assi, "Demand-side management by regulating charging and discharging of the EV, ESS, and utilizing renewable energy," *IEEE Trans. Ind. Inform.*, vol. 14, no. 1, pp. 117–126, Jan. 2018.

[6] M Shakeri *et al.*, "An overview of the building energy management system considering the demand response programs, smart strategies and smart grid," *Energies*, vol. 13, no. 13, 2020, Art. no. 3299.

[7] M H Dadashi-Rad *et al.*, "Modeling and planning of smart buildings energy in power system considering demand response," *Energy*, vol. 213, no. C, 2020, Art. no. 118770.

[8] F. Wang *et al.*, "Multi-objective optimization model of source-load-storage synergetic dispatch for a building energy management system based on TOU price demand response," *IEEE Trans. Ind. Appl.*, vol. 54, no. 2, pp. 1017–1028, Mar./Apr. 2018.
[9] R. Teng and T. Yamazaki, "Load profile-based coordination of appliances in a smart home," *IEEE Trans. Consum. Electron.*, vol. 65, no. 1, pp. 38–46, Feb. 2019.
[10] Y. Liu, L. Xiao, G. Yao, and S. Bu, "Pricing-based demand response for a smart home with various types of household appliances considering customer satisfaction," *IEEE Access*, vol. 7, pp. 86463–86472, 2019.
[11] F. Luo, W. Kong, G. Ranzi, and Z. Y. Dong, "Optimal home energy management system with demand charge tariff and appliance operational dependencies," *IEEE Trans. Smart. Grid.*, vol. 11, no. 1, pp. 4–14, Jan. 2020.
[12] Y. Wang *et al.*, "Economic and efficient multi-objective operation optimization of integrated energy system considering electro-thermal demand response," *Energy*, vol. 205, no. C, 2020, Art. no. 118022.
[13] C. Ju, P. Wang, L. Goel, and Y. Xu, "A two-layer energy management system for microgrids with hybrid energy storage considering degradation costs," *IEEE Trans. Smart Grid*, vol. 9, no. 6, pp. 6047–6057, Nov. 2018.
[14] F. Luo, G. Ranzi, S. Wang, and Z. Y. Dong, "Hierarchical energy management system for home micro-grids," *IEEE Trans. Smart. Grid.*, vol. 10, no. 5, pp. 5536–5546, Sep. 2019.
[15] S. Sharma, Y. Xu, A. Verma, and B. K. Panigrahi, "Time-coordinated multi-energy management of smart buildings under uncertainties," *IEEE Trans. Ind. Inform.*, vol. 15, no. 8, pp. 4788–4798, Aug. 2019.
[16] M. Shafie-Khah and P. Siano, "A stochastic home energy management system considering satisfaction cost and response fatigue," *IEEE Trans. Ind. Inform.*, vol. 14, no. 2, pp. 629–638, Feb. 2018.
[17] Z. Li, Y. Xu, S. Fang, X. Zheng, and X. Feng, "Robust coordination of a hybrid AC/DC multi-energy ship microgrid with flexible voyage and thermal loads," *IEEE Trans. Smart. Grid*, vol. 11, no. 4, pp. 2782–2793, Jul. 2020.
[18] S. Sharma, A. Verma, Y. Xu, and B. K. Panigrahi, "Robustly coordinated bi-level energy management of a multi-energy building under multiple uncertainties," *IEEE Trans. Sustain. Energy*, vol. 12, no. 1, pp. 3–13, Jan. 2021.
[19] C. Zhang *et al.*, "Affinely adjustable robust energy management system for smart homes," *IET Renewable Power Gener.*, vol. 14, no. 15, pp. 2955–2965, Nov. 2020.
[20] W. Wei, F. Liu, and S. Mei, "Distributionally robust co-optimization of energy and reserve dispatch," *IEEE Trans. Sustain. Energy*, vol. 7, no. 1, pp. 289–300, Jan. 2016.
[21] P. Zhao, C. Gu, D. Huo, Y. Shen, and I. Hernando-Gil, "Two-stage distributionally robust optimization for energy hub systems," *IEEE Trans. Ind. Inform.*, vol. 16, no. 5, pp. 3460–3469, May 2019.
[22] Y. Zhou, M. Shahidehpour, Z. Wei, Z. Li, G. Sun, and S. Chen, "Distributionally robust unit commitment in coordinated electricity and district heating networks," *IEEE Trans. Power Syst.*, vol. 35, no. 3, pp. 2155–2166, May 2020.
[23] M. Daneshvar, B. Mohammadi-Ivatloo, K. Zare, and S. Asadi, "Two-stage robust stochastic model scheduling for transactive energy-based renewable microgrids," *IEEE Trans. Ind. Inform.*, vol. 16, no. 11, pp. 6857–6867, Nov. 2020.
[24] J. Zhong *et al.*, "Distributed operation for integrated electricity and heat system with hybrid stochastic/robust optimization," *Int. J. Electr. Power Energy Syst.*, vol. 128, 2021, Art. no. 106680.
[25] A. Dini *et al.*, "Hybrid stochastic/robust scheduling of the grid-connected microgrid based on the linear coordinated power management strategy," *Sustain. Energy, Grids Netw.*, vol. 24, no. 3, 2020, Art. no. 100400.
[26] S. Sharma, A. Verma, and B. K. Panigrahi, "Robustly coordinated distributed voltage control through residential demand response under multiple uncertainties," *IEEE Trans. Ind. Appl.*, vol. 57, no. 4, pp. 4042–4058, Jul./Aug. 2021.
[27] Z. Li, Y. Xu, L. Wu, and X. Zheng, "A risk-averse adaptively stochastic optimization method for multi-energy ship operation under diverse uncertainties," *IEEE Trans. Power Syst.*, vol. 36, no. 3, pp. 2149–2161, May 2021.
[28] L. Wang *et al.*, "Non-cooperative game-based multilateral contract transactions in power-heating integrated systems," *Appl. Energy*, vol. 268, no. C, 2020, Art. no. 114930.
[29] Y. Chen *et al.*, "Optimally coordinated dispatch of combined-heat-and-electrical network with demand response," *IET Gener., Transmiss. Distrib.*, vol. 13, no. 4, pp. 2216–2225, 2019.
[30] Z. Li, Y. Xu, X. Feng, and Q. Wu, "Optimal stochastic deployment of heterogeneous energy storage in a residential multi-energy microgrid with demand-side management," *IEEE Trans. Ind. Inform.*, vol. 17, no. 2, pp. 991–1004, Feb. 2021.
[31] A. Ahmadi, A. E. Nezhad, and B. Hredzak, "Security-constrained unit commitment in presence of lithium-ion battery storage units using information-gap decision theory," *IEEE Trans. Ind. Inform.*, vol. 15, no. 1, pp. 148–157, Jan. 2019.
[32] Z. Li, L. Wu, and Y. Xu, "Risk-averse coordinated operation of a multi-energy micro-grid considering voltage/var control and thermal flow: An adaptive stochastic approach," *IEEE Trans. Smart Grid*, vol. 12, no. 5, pp. 3914–3927, Sep. 2021.
[33] B. Zhou *et al.*, "Optimal scheduling of virtual power plant with battery degradation cost," *IET Gener. Trans. Distrib.*, vol. 10, no. 3, pp. 712–725, 2016.
[34] K. Lai and M. S. Illindala, "Sizing and siting of distributed cloud energy storage systems for a shipboard power system," *IEEE Trans. Ind. Appl.*, vol. 57, no. 3, pp. 1935–1944, May/Jun. 2021.
[35] P. Li, C. Zhang, Z. Wu, Y. Xu, M. Hu, and Z. Dong, "Distributed adaptive robust voltage/VAR control with network partition in active distribution networks," *IEEE Trans. Smart Grid,* vol. 11, no. 3, pp. 2245–2256, May 2019.
[36] "Supplementary information for the case study," Dec. 2021. Available [Online]: [Online]. Available: https://www.dropbox.com/s/xs8oy4onx8rgjfc/Supplementary%20information%20for%20the%20Case%20Study.pdf?dl=0
[37] Y. Wang, Y. Tang, Y. Xu, and Y. Xu, "A distributed control scheme of thermostatically controlled loads for the building-microgrid community," *IEEE Trans Sustain. Energy*, vol. 11, no. 1, pp. 350–360, Jan. 2020.

Zhengmao Li (Member, IEEE) received the B.E. degree in information engineering and the M.E. degree in electrical engineering from Shandong University, Jinan, China, in 2013 and 2016, respectively, and the Ph.D. degree in electrical engineering from the School of Electrical and Electronic Engineering, Nanyang Technological University, Singapore, in 2020. During 2019—2021, he was a Research Fellow with the Stevens Institute of Technology, Hoboken, NJ, USA, and he is currently a Research Fellow with Nanyang Technological University under the NTU-ETH Project. His research interests include renewable energy integration, microgrid and multi-energy system, and optimization techniques such as approximate dynamic programming, robust optimization, and stochastic optimization.

Lei Wu (Senior Member, IEEE) received the B.S. degree in electrical engineering and the M.S. degree in systems engineering from Xi'an Jiaotong University, Xi'an, China, in 2001 and 2004, respectively, and the Ph.D. degree in electrical engineering from the Illinois Institute of Technology (IIT), Chicago, IL, USA, in 2008. From 2008 to 2010, he was a Senior Research Associate with the Robert W. Galvin Center for Electricity Innovation, IIT. In 2012, he was a summer Visiting Faculty with NYISO. He was a Professor with Electrical and Computer Engineering Department, Clarkson University, Potsdam, NY, USA, till 2018. He is currently a Professor with the Electrical and Computer Engineering Department, Stevens Institute of Technology, Hoboken, NJ, USA. His research interests include power systems operation and planning, energy economics, and community resilience microgrid.

Yan Xu (Senior Member, IEEE) received the B.E. and M.E degrees in electrical engineering from the South China University of Technology, Guangzhou, China, in 2008 and 2011, respectively, and the Ph.D. degree in electrical engineering from The University of Newcastle, Callaghan, NSW, Australia, in 2013. He is currently the Nanyang Associate Professor with the School of Electrical and Electronic Engineering, Nanyang Technological University (NTU), Singapore, and a Cluster Director of Energy Research Institute at NTU, Singapore. Previously, he held The University of Sydney Postdoctoral Fellowship in Australia. His research interests include power system stability and control, microgrid, and data analytics for smart grid applications. Dr. Xu is currently the Editor of the IEEE TRANSACTIONS ON POWER SYSTEMS, IEEE TRANSACTIONS ON SMART GRID, IEEE Power Engineering Letters, *CSEE Journal of Power and Energy Systems*, and an Associate Editor for the *IET Generation, Transmission and Distribution*.

Xiaodong Zheng (Member, IEEE) received the B.S. degree in electrical engineering from the South China University of Technology, Guangzhou, China, in 2015, and the Ph.D. degree in electrical engineering from the same institute in 2020. From 2018 to 2019, he was a Research Assistant with Nanyang Technological University, Singapore. Prior to that, he was a Joint Graduate Student with the Power Dispatching and Control Center of China Southern Grid Company, Ltd., China, from 2015 to 2017.